Quantitative perfusion mapping with induced transient hypoxia using BOLD MRI

Chau Vu, Yaqiong Chai, Julie Coloigner, Aart J Nederveen, Matthew Borzage, Adam Bush, John C Wood

Quantitative Perfusion Mapping with Induced Transient Hypoxia using BOLD MRI

Chau Vu,[1] Yaqiong Chai,[1,2] Julie Coloigner,[2,3] Aart J. Nederveen,[4] Matthew Borzage,[5,6] Adam Bush,[7] John C. Wood[1,8,*]

[1]Department of Biomedical Engineering, University of Southern California, Los Angeles, CA 90007, USA
[2]CIBORG Laboratory, Division of Radiology, Children's Hospital Los Angeles, Los Angeles, CA 90027, USA
[3]Univ Rennes, CNRS, Inria, Inserm, IRISA UMR 6074, Empenn ERL U 1228, F-35000 Rennes, France
[4]University of Amsterdam, Amsterdam UMC, Radiology and Nuclear Medicine, the Netherlands
[5]Division of Neonatology, Fetal and Neonatal Institute, Children's Hospital Los Angeles, Los Angeles, CA 90027, USA
[6]Department of Pediatrics, Keck School of Medicine, University of Southern California, Los Angeles, CA 90007, USA
[7]Department of Radiology and Department of Electrical Engineering, Stanford University, Stanford, CA 94305, USA
[8]Division of Cardiology, Departments of Pediatrics and Radiology, Children's Hospital Los Angeles, Los Angeles, CA 90027, USA

*** Correspondence to:**
Dr. John C. Wood
Division of Cardiology, Mailstop 34
Children's Hospital Los Angeles
4650 Sunset Blvd
Los Angeles, CA 90027-0034
(323) 361-5470
jwood@chla.usc.edu

Running head: Perfusion mapping with transient hypoxia

Submission type: Full paper

Paper word count: 4800

Abstract word count: 225

Number of tables: 3

Number of figures: 6

Number of references: 66

Abstract:

Purpose: Gadolinium-based dynamic susceptibility contrast (DSC) is commonly used to characterize blood flow in patients with stroke and brain tumors. Unfortunately, gadolinium contrast administration has been associated with adverse reactions and long-term accumulation in tissues. In this work, we propose an alternative deoxygenation-based dynamic susceptibility contrast (dDSC) method that uses a transient hypoxia gas paradigm to deliver a bolus of paramagnetic deoxygenated hemoglobin to the cerebral vasculature for perfusion imaging.

Methods: Through traditional DSC tracer kinetic modeling, the MR signal change induced by this hypoxic bolus can be used to generate regional perfusion maps of cerebral blood flow, cerebral blood volume and mean transit time. This gas paradigm and BOLD-MR imaging were performed concurrently on a cohort of 66 healthy and chronically anemic subjects (age 23.5±9.7, female 64%).

Results: Our results showed reasonable global and regional agreement between dDSC and other flow techniques like phase contrast and arterial spin labeling.

Conclusion: In this proof-of-concept study, we demonstrated the feasibility of using transient hypoxia to generate a contrast bolus that mimics the effect of gadolinium and yields reasonable perfusion estimates. Looking forward, optimization of the hypoxia boluses and measurement of the arterial-input-function is necessary to improve the accuracy of dDSC. Additionally, a cross-validation study of dDSC and DSC in brain tumor and ischemic stroke subjects is warranted to evaluate the clinical diagnostic utility of this approach.

Keywords: dynamic susceptibility contrast, transient hypoxia, deoxyhemoglobin contrast, phase contrast, arterial spin labeling

1. Introduction:

Gadolinium-based dynamic susceptibility contrast (DSC) imaging is the most commonly used methodology to assess cerebral perfusion and characterize tumor hemodynamics in clinical studies.[1] With the injection of a gadolinium exogenous contrast, DSC utilizes a series of echo-planar gradient-echo acquisitions to monitor the first pass of this contrast bolus through the capillary beds and derives an assortment of cerebral perfusion metrics, including cerebral blood flow (CBF), cerebral blood volume (CBV) and mean transit time (MTT).[2] The strength of this technique lies in its high temporal resolution to capture the bolus passage through brain tissue on the order of a few seconds and its ability to generate hemodynamic information within the same scan. In the last few decades, DSC has proven to be a valuable tool for evaluation of ischemic and infarcted tissues in stroke,[3] differential diagnosis of intracranial masses[4] and assessment of blood-brain barrier permeability in traumatic brain injury.[5]

However, despite its utility in numerous clinical applications, DSC is limited by its reliance on various gadolinium-based contrast agents, each of which has a known or hypothetical association with nephrogenic systemic fibrosis in patients with kidney disease.[6,7] Even in patients with normal renal function, gadolinium agents have been demonstrated to accumulate in tissues in the brain, bone and kidney.[8–10]

In recent years, oxygen has been employed as a safer alternative to exogenous contrast[11] since the over-supply (hyperoxia) or the lack of oxygen (hypoxia) can change the blood oxygen content, modulate the deoxyhemoglobin concentration and cause a T2-weighted change of the measured MR signal. MacDonald et al. have previously demonstrated the use of hyperoxia-induced signal dynamics to estimate perfusion parameters.[12] However, Losert et al. showed hyperoxia causes a relatively small increase in oxygen saturation and percent signal change in the white matter (less than 1%),[11] which prevents accurate flow measurement and examination of the role of compromised CBF in white matter disease.[13] Therefore, we conjectured that briefly increasing the concentration of paramagnetic deoxyhemoglobin via desaturation would produce a larger and more robust signal change, especially in the white matter.

In this study, we explored the feasibility of using a transient hypoxia gas paradigm, in a similar manner to gadolinium injection, to deliver a bolus of paramagnetic material

(deoxygenated hemoglobin) to the cerebral vasculature. The contrast passage through the microvasculature was monitored by a dynamic blood-oxygen-level-dependent (BOLD) MR sequence. Through tracer kinetics modeling, the BOLD signal change induced by this hypoxic bolus can be used to generate regional perfusion maps; we term this approach deoxygenation-based DSC (dDSC). In order to test the new technique over a wide range of CBF, we evaluated this technique on a total of 66 subjects, including healthy controls as well as anemic patients (sickle cell disease and non-sickle anemia) who have higher baseline blood flow.[14,15] Comparison with other popular CBF quantification methods such as arterial spin labeling (ASL)[16] and phase contrast (PC)[17] can yield further insights into the feasibility of using transient hypoxia as a contrast mechanism for dDSC perfusion studies.

2. Methods:

2.1. Theory:

In DSC imaging, the changes in relaxation rate $\otimes R_2^*$ are directly proportional to the gadolinium concentration.[18,19] In parallel, this dDSC approach assumes that the changes of oxygen level in the brain can be approximated by a linear function of $\otimes R_2^*$ during the gas paradigm:

$$C_{tissue}(t) = kR_2^* \quad [1]$$

where $C_{tissue}(t)$ is the oxygen concentration time curve measured in the tissue and k is a proportionality constant that depends on tissue type, contrast agent, field strength and pulse sequence.[20] In this experiment design, voxel-wise $\otimes R_2^*$ is calculated with:

$$R_2^*(t) = -\frac{1}{TE} ln\left(\frac{S(t)}{S_0}\right) \quad [2]$$

where $S(t)$ is the gradient-echo time series, S_0 is the baseline signal computed from the first 25 dynamics prior to bolus administration and TE is the echo time. Arterial input function (AIF) and venous output function (VOF) are extracted from the middle cerebral artery (Figure 3A) the superior sagittal sinus (Figure 3B) respectively. Due to difficulty extracting a pure intravascular blood signal from the middle cerebral artery because of partial volume effect,[21] the time integral of the AIF is scaled to match that of the VOF[22] to yield an 'effective AIF' signal $eAIF(t)$ such that:

$$\int \quad R^*_{2_{eAIF}}(t) = \int_{\blacksquare}^{\blacksquare} R^*_{2_{VOF}}(t)$$

[3]

Regional CBV is computed using $\otimes R_2^*$ from the tissue and effective AIF:

$$CBV = \frac{\kappa}{\rho} \frac{\int_{\blacksquare}^{\blacksquare} R^*_{2_{tissue}}(t)}{\int_{\blacksquare}^{\blacksquare} R^*_{2_{eAIF}}(t)}$$

[4]

where ρ is the brain density 1.05g/mL and κ is the hematocrit correction factor. The measure $\kappa = \frac{1-Hct}{1-0.69Hct}$ accounts for the difference between the hematocrit in the large vessels (middle cerebral artery for AIF determination) and in the microvasculature.[23] From tracer kinetics modeling, the measured $C_{tissue}(t)$ is expressed as:

$$C_{tissue}(t) = eAIF(t) \otimes (CBF \times R(t)) \qquad [5]$$

where $R(t)$ is the residue function of the contrast fraction present in the vasculature at time t with $R(0) = 1$ and $R(\infty) = 0$.[18] To compute CBF, a deconvolution can be performed by an inverse Fourier transform approach[24] or a singular value decomposition (SVD) method proposed by Ostergaard et al.[25] Stable solutions for inverse discrete Fourier transforms can only be obtained with effective experimental noise suppression, whereas SVD has been shown to reproduce flow and is independent of underlying vasculature and volume.[25] In this study, we used the SVD deconvolution approach, with the previous convolution discretized in the following form:

$$[C_{tissue}(t_1)\ C_{tissue}(t_2)\ \vdots\ C_{tissue}(t_N)\ ] =$$
$$t\ [eAIF(t_1)\ 0\ \dots\ 0\ eAIF(t_2)\ eAIF(t_1)\ \dots\ 0\ \dots\ \dots\ \dots\ \dots\ eAIF(t_N)\ eAIF(t_{N-1})\ \dots\ eAIF(t_1)\ ]\ [CBF \times R(t_1)\ CBF \times R(t_2)\ \vdots\ CBF \times R(t_N)\ ] \qquad [6]$$

After fitting $CBF \times R(t)$ with SVD, CBF is determined as the initial height of this tissue response function. Finally, MTT is calculated as a direct ratio between regional CBV and CBF:

$$MTT = \frac{CBV}{CBF} \qquad [7]$$

2.2. Study protocol:

The Committee on Clinical Investigation at Children's Hospital Los Angeles (CHLA) approved the protocol; written informed consent and/or assent were obtained

from all subjects (CCI#2011-0083). This study was performed in accordance with the Declaration of Helsinki.

A total of 66 subjects were tested between April 2012 and December 2017. This cohort was divided into two patient groups: 28 healthy controls and 38 chronically anemic patients (including sickle cell anemia, thalassemia and other anemia syndromes). Exclusion criteria were prior neurologic insult, pregnancy, acute chest or pain crisis hospitalization within one month and major medical problems outside of their chronic anemia. Only subjects older than 12 years of age were included in the study. Imaging, vital signs and blood samples were obtained on the same day for each subject. Complete blood count was analyzed in our clinical laboratory. Demographic and clinical variables of each patient group are summarized in Table 1.

2.3. Transient hypoxia:

Figure 1 illustrates the experimental setup for the respiratory challenge MRI. At the start of the image acquisition, patients were breathing through a custom, two-liter reservoir rebreathing circuit supplied by pressurized, non-humidified room air (21% oxygen, balanced nitrogen) at 12 liters per minute. This system included one-way valves to prevent partial gas mixtures and respiratory bellows (Invivo Corporation, Gainesville, FL) to display the breathing pattern and frequency. At 50 seconds into the data acquisition, the room air gas mixture was switched to 100% nitrogen until the patient had completed 5 breaths (approximately 25 seconds, counted through the respiratory bellows data display), then the circuit was changed back to room air. This previously-developed protocol[26] caused a safe and short desaturation; typical desaturations had a minimum S_pO_2 of 75-80%. The pulse oximetry measurements during transient hypoxia (Figure 2A) demonstrated similar depth and duration to spontaneous desaturations (Figure 2B). More details on this protocol are provided in Supporting Information Methods section.

2.4. Magnetic resonance imaging acquisition:

Each participant underwent an MRI study using a 3T Philips Achieva using an 8-element phased-array coil. Anatomical 3D T1, BOLD, phase contrast and arterial spin labeling scans were performed in all subjects prior to transient hypoxia.

For each subject, a 3D T1-weighted image was acquired with TR = 8.20ms, TE = 3.8ms, flip angle = 8°, resolution = 1×1×1mm and FOV = 256×224×160mm. BOLD-MR images were acquired with the following parameters: TR = 2000ms, TE = 50ms, flip angle = 90°, resolution = 2.5×2.5×5mm and FOV = 220×220×130m. A total of 150 volumes were collected. Phase contrast images were obtained, positioned just above the carotid bifurcation with the following parameters: TR = 12.9ms, TE = 7.7ms, flip angle = 10°, resolution = 1.3×1.3×5mm, FOV = 240×261×5mm and velocity encoding gradient of 100cm/s. Pseudo continuous ASL scans were performed using an unbalanced Hanning shaped RF pulse labeling train (mean gradient 1G/cm, interpulse interval of 1ms, pulse duration 0.5ms) and a 3D GRASE two-shot readout scheme with the following parameters: TR = 3800ms, TE = 9.8ms, resolution = 3.7×3.7×10mm, labeling duration = 2000ms, post-labeling delay = 1600ms, dynamics = 10 and EPI factor = 5. Two inversion pulses for background suppression were used, with an inversion efficiency of 95% each. All MR acquisition parameters have been detailed in prior publications.[13,27]

2.5. Image pre-processing:

The phase contrast images were analyzed using an in-house MATLAB program (Mathworks, Natick, MA). Stationary tissue pixels were identified in the complex difference images by simple thresholding using a mean plus two standard deviations from a remote, nonvascular region. Phase differences of stationary pixels were fit to a second-order two-dimensional polynomial and used to remove the background phase from vessels. Vessel boundaries were identified semi-automatically from the complex difference image processed using a Canny edge-detector. A single-voxel dilation of vessel boundaries was then performed, and only voxels whose complex difference was greater than the stationary tissue threshold was retained. Finally, CBF (mL/100g/min) was computed with $CBF = \sum_i^{\blacksquare} \blacksquare A_i \times V_i$, where A_i is the area and V_i is the velocity defined by PC-MRI of each voxel. Total CBF, which was the sum of the flow in the left and right internal carotid arteries and vertebral arteries, was corrected for total grey and white matter volume assuming a brain density of 1.05g/mL.

The ASL images were rigidly registered to T1-weighted images and then to Montreal Neurological Institute (MNI) template using FMRIB Software Library (FSL).[28]

Regional CBF quantification was performed using a two-compartment kinetic model[13] and estimates of labeling efficiency, disease-specific blood T1 and tissue-specific arterial transit times. A comprehensive discussion of these parameters was detailed in our previous publications.[13,29]

The BOLD images were preprocessed with FSL using a standard spatial functional pipeline. Images were first slice-time corrected, realigned to remove physiological motion and then co-registered to the MNI template space. Finally, the registered volumes were normalized and smoothed using 8×8×8mm Gaussian kernel similar to typical pre-processing for BOLD fMRI datasets.[30,31] More details of this preprocessing pipeline are described in previous publication.[27] Percentage change of the MR signal *ΔBOLD* is calculated as $\Delta BOLD = \frac{BOLD_{hypoxia} - BOLD_{baseline}}{BOLD_{baseline}} \times 100\%$ (Figure 2C), where $BOLD_{hypoxia}$ was the nadir of the hypoxic time curve and $BOLD_{baseline}$ was the average of volumes [5, 25] out of 150 temporal volumes.

To minimize the partial volume effects, the AIF was rescaled by the time integral of the VOF measured at the superior sagittal sinus[22,32] (refer to Methods section 2.1) since the superior sagittal sinus is a large, long and straight lumen parallel to the main magnetic field and less vulnerable to partial volume errors. The AIF and VOF were extracted from BOLD images that had been motion-corrected but neither smoothed nor registered to the MRI template. Localizations of the middle cerebral artery and the superior sagittal sinus were done using a previously published technique on a simple difference dataset of $BOLD_{difference} = BOLD_{baseline} - BOLD_{hypoxia}$ (Figure 3).[33] The transient hypoxia model was approximated with a linear function during the rise time of the desaturation bolus and an exponential decay function during the signal recovery; the pre-hypoxia and post-hypoxia baselines were modeled as constants (Figure 2D). To avoid the effects of recirculation and hyperemia as confounders, the end-point of the exponential decay was determined by minimizing the least-square error, and the area under the curve was only computed under the linear and exponential portions using the Riemann sum integration approach.

From these datasets, perfusion maps for CBF, CBV and MTT maps were computed using an in-house MATLAB program (Mathworks, Natick, MA). Grey matter and white matter perfusion values were computed as an average within tissue-specific

masks derived from an average of 152 T1-weighted MRI scans in the common MNI coordinate system.[34] White matter masks were eroded by two voxels to minimize partial volume effects. Since cerebral perfusion measurements have a bimodal distribution, values were reported for grey matter and white matter separately. Masks of the anterior cerebral artery (ACA), middle cerebral artery (MCA) and posterior cerebral artery (PCA) circulations in the grey matter were based on the published templates of vascular territories in both hemispheres.[35] The territories were created from anatomic studies of cerebral vascularization and evaluated on the bicommissural plane.

2.6. Statistical analysis:

Statistical analysis on global desaturation values was performed in JMP (SAS, Cary, NC). Student's *t*-test was used to examine the difference in clinical variables between the two study groups. Paired *t*-tests were used to compare CBF computed using dDSC, ASL and phase contrast. Correlation tests and Bland-Altman analyses were performed to assess global and regional agreement between different flow measures. Adherence to the *a priori* transient hypoxia model of linear rise and exponential decay was calculated with the root-mean-square percentage error (RMSPE) as $RMSPE = \sqrt{\frac{\left[\sum_{i=1}^{n} \frac{y_i - \hat{y}_i}{y_i}\right]^2}{n}} \times 100\%$, where *n* is the total number of sample points, y_i is the actual signal and $\hat{y}_i$ is the predicted signal.

3. Results:

All 66 subjects completed T1, BOLD, phase contrast and ASL imaging. When this study first started, we were initially unable to perform ASL compatible with the White Paper[16] until October 2014, thus comparative ASL images were available in only 45 out of 66 subjects. Additionally, four additional ASL datasets were excluded due to motion, leaving 16 control and 25 anemic subjects in the ASL analysis (Table 1). There were no differences in the demographic and hematologic data between the complete cohort and the cohort after subject exclusion in the ASL analysis.

3.1. Quality of AIF and VOF vessels:

Localizations of the AIF from the middle cerebral artery and the VOF from the superior sagittal sinus are shown in a representative subject in Figure 3. Time integral of the normalized venous signal was 140% stronger in magnitude compared to the raw AIF signal in all subjects. Scaling of the AIF by the VOF yielded an average CBF of 42.4±18.6 mL/100g/min and an average CBV of 4.8±1.3 mL/100g in healthy controls within the acceptable range in literature.

3.2. Perfusion measured by deoxygenation-based DSC:

None of the patients consciously perceived the hypoxia episode and no complications were encountered. This gas paradigm produced an average drop of 16.5±9.0% in S_pO_2 and of 4.3±1.7% and 7.9±2.8% in BOLD signal in the white matter and grey matter respectively compared to baseline. Table 2 summarizes average perfusion values in the grey matter and white matter separately for two patient groups, with anemic patients showing significantly higher CBF and CBV compared to healthy controls. Moreover, anemic patients also had slightly faster transit time compared to healthy patients.

Figure 4 shows a trend of agreement between CBF values derived from dDSC, phase contrast and ASL. There is a systemic underestimation of 20.0 mL/100g/min by dDSC compared to phase contrast with large limits of agreement, and a smaller bias of 12.0 mL/100g/min compared to ASL in the Bland-Altman analysis. MTT was also well-correlated with CBF in hypoxia-based and phase contrast methods (r^2=0.25, p<0.01 and r^2=0.13, p=0.03 respectively) but only trended for ASL (r^2=0.08, p=0.08). Higher perfusion values were negatively correlated with age (r^2=0.11, p=0.01) but not with sex (p=0.77). Additionally, lower hemoglobin levels were associated with higher CBF and CBV (r^2=0.29, p<0.01 and r^2=0.17, p<0.01 respectively) and with lower MTT (r^2=0.11, p<0.01).

In addition to global analysis, voxel-wise perfusion maps were also generated for the hypoxia-based perfusion method (Figure 5). RMSPE maps in Figure 5D demonstrated strong adherence to the *a priori* hypoxia model of linear rise and exponential decay, demonstrating robust desaturation observable in voxels across the brain. In addition to group average perfusion maps, examples of individual perfusion maps were also illustrated for two control and two anemic subjects in Supporting Information Figure S1.

Test-retest was performed in two healthy control subjects, with individual values shown in Supporting Information Table S1 and individual maps in Supporting Information Figure S2.

Regional analysis of perfusion within three arterial territories is detailed in Table 3. Even though the middle cerebral arteries' territory showed a trend of higher blood flow and faster transit time compared to the anterior and posterior cerebral arteries, one-way ANOVA tests demonstrated no significant difference between perfusion in the three territories (p=0.54 for CBF, p=0.07 for CBV, p=0.83 for MTT). CBF and CBV maps also showed significantly higher values in the grey matter compared to the white matter (p<0.01), with the average grey–white matter ratio of 1.4 for CBV and 1.5 for CBF – lower than the grey–white ratio of 1.9 in ASL maps. Similarly, MTT map demonstrated grey–white matter differentiation (p=0.01), but the distinction was not as strong and more confined to the deep white matter tissue.

Furthermore, regional correlation analysis between CBF_{dDSC} and CBF_{ASL} (Figures 4C and 4E) demonstrated a good association within the grey matter but not in the white matter. Even though imprecise registration prevented voxel-wise comparison between the two approaches, the ACA, MCA and PCA vascular territories within the grey matter all demonstrated reasonable agreement between CBF estimates by dDSC and ASL techniques (Figures 6A, 6C and 6E). There is no significant bias in perfusion measurements by dDSC compared to ASL in different vascular territories of the brain in the Bland-Altman analyses (Figures 6B, 6D and 6F).

4. Discussion:

Our hypoxia protocol induced a reproducible drop in MR signal in both control and anemic patients similar to the mechanism of gadolinium-based DSC. However, unlike DSC, the signal loss in dDSC was smaller in magnitude and induced by increased paramagnetic deoxygenated hemoglobin, leading to shorter T2* and lower gradient-echo signal. While other gas paradigms such as 100% oxygen had been used to investigate baseline perfusion in healthy subjects,[12] this work represented the first study to use transient hypoxia as a contrast method for CBF quantification. It is also the first to show a reasonable trend of agreement between dDSC perfusion values and independent flow

techniques like ASL and phase contrast. Additionally, the physiologic associations between dDSC with age and hemoglobin were expected and provided an extra layer of reassurance for our data quality.

This novel dDSC technique offers many advantages over conventional gadolinium-based DSC. In eliminating the need for an exogenous contrast medium, this method offers an alternative contrast that is well-tolerated, repeatable, does not lead to anaphylaxis and is convenient in patients whose venous access is more challenging, such as in pediatric or anemic subjects. This method is significantly cheaper compared to gadolinium as well as iron-based contrast like ferumoxytol. It is also potentially easily translatable to clinical protocols, especially for perfusion quantification in patients under anesthesia. Apart from brain imaging, since previous work has demonstrated good performance of BOLD imaging and different respiratory challenges in the liver, kidney and heart,[36–39] this dDSC technique can potentially be applied to assess in these organs where non-contrast imaging modalities like ASL have proven less effective due to low signal-to-noise ratio.[40]

Most importantly, this hypoxia gas paradigm is very safe and well-tolerated; our laboratory has performed this experiment on over 200 subjects in a larger study on sickle cell anemia without any major adverse events such as stroke or transient ischemic attack.[26,41] In a review on the safety of hypoxia challenges, Bickler et al. showed that hypoxia experiments have been performed at many different research centers across the world with arterial saturations dropping as low as 45%, which is considerably lower than the typical hypoxia levels experienced in our study.[42] Overall, these brief exposures to hypoxia have been demonstrated to be well-tolerated without any evidence of cardiovascular compromise, systemic acidosis or lasting cognitive impairment.[42]

Absolute quantification of CBF is difficult due to the large partial volume effects in the AIF related to small vessel sizes and limited spatial resolution.[43] While many multiplicative rescaling methods for AIF correction have been explored,[44] rescaling with a VOF from the superior sagittal sinus has proven robust due to the large vessel caliber of the superior sagittal sinus as well as its position parallel to the magnetic field and orthogonal to the imaging plane.[32,45] However, even with the use of venous rescaling, our CBV measurement was still overestimated compared to normal literature values.

Additionally, even though phase contrast has been shown to overestimate total blood flow,[46] the large bias between CBF measured by dDSC and phase contrast might be due to the low quality of the AIF. AIF which were contaminated with nearby tissue voxels was lower and broader in shape, leading to lower CBF values.[47] Partial volume effects were still present in the superior sagittal sinus, leading to lower area-under-curve of the VOF and AIF and consequently to overestimation of tissue CBV. Heterogenous and low quality of AIF was the potential cause for large limits of agreement of dDSC compared to phase contrast and ASL. An overestimation of CBV and underestimation of CBF led to a systematic overestimation of MTT in this study. Future work to employ alternative and more effective methods to extract the AIF and VOF will be necessary to improve the accuracy of CBV and CBF measurements in dDSC.

In general, CBF_{dDSC} showed reasonable inter-modality agreement with phase contrast and ASL using correlation and Bland-Altman analyses. The stronger correlation between CBF_{dDSC} with phase contrast compared to ASL was understandable since phase contrast is independent of T1 and T2 relaxations and has relatively high signal-to-noise ratios. In addition to the agreement in whole-brain blood flow, our dDSC-based CBF measures also showed regional agreement with ASL perfusion maps. Grey matter as well as the three vascular territories all displayed more robust inter-modality association between CBF_{dDSC} and CBF_{ASL} compared to deep white matter regions, suggesting a divergence in the sensitivities of these two methods to microvascular perfusion characteristics in the white matter.

Our observation of significantly higher blood flow and volume in anemic patients compared to healthy controls was consistent with previous works showing increased baseline perfusion in compensation for compromised oxygen carrying capacity in chronic anemia.[14,15] The faster MTT in anemic patients was also in accordance with the shorter vascular transit times measured with multi-post-labeling delay ASL.[48] Shorter MTT in anemic subjects was apparent in the grey matter as well as regions of normally perfused white matter; however, these subjects also displayed abnormally slower contrast dynamics in the deep white matter at the end of the perfusion branches. These borderzone regions coincided with typical watershed areas of flow limitation and peak oxygen extraction[13,49] and were consistent with previous studies that showed reduced

flow reserve in areas vulnerable to silent strokes,[50] suggesting a connection between hemodynamic impairment and the development of strokes in anemic patients.

Even though ASL is the prominent non-invasive perfusion technique and has been the focus of much research and development in the MRI community, ASL is still hampered by some disadvantages compared to dDSC. Most notably ASL has low signal-to-noise ratio in the white matter, possibly contribution to the lack of agreement between white matter CBF measured by the two techniques. Additionally, ASL is confounded by model assumptions and physical parameters including blood T1 and arterial transit time, many of which are different in anemic patients compared to healthy controls.[29] Blood T1 can be measured with T1-mapping,[51,52] but measurement of arterial T1 remains challenging and not universally available. Arterial transit time confounds can also be avoided by utilizing multiple post-labeling delay ASL,[16] but there is currently too much heterogeneity in the acquisition techniques. Additionally, simple multi-delay ASL can take significantly longer than single-delay ASL. Acceleration methods such as Hadamard encoding or Look-Locker readouts can be used to shorten acquisition time, but these are typically unavailable on routine clinical scanners. Therefore, even though ASL will undoubtedly have an important place in the future of perfusion imaging, the development of this novel dDSC technique provides an alternative and generalizable method for measuring tissue blood flow and builds upon the previous work that has already been pioneered by the perfusion MRI community.

An important assumption in our dDSC model was the linearity between cerebral oxygen level and the changes in MRI signal $\otimes R_2^*$ during the hypoxia gas paradigm in equation [1]. Calibrated BOLD model typically presents a non-linear relationship between deoxygenated hemoglobin and changes in the BOLD signal with a vessel size-dependent parameter β = 1.3 at 3T.[53] However, under hypoxic conditions, in addition to capillaries and venules, larger deoxygenated arterioles also contribute to the BOLD signal, in which case β is likely decreased closer to 1 and the relationship between the BOLD signal and oxygen saturation could be approximated with a linear function. Furthermore, previous work by Rostrup et al. has demonstrated an approximately linear relationship between $\otimes R_2^*$ and oxygen saturation during hypoxic exposure, thus confirming that the linearity assumption was reasonable.[54] Future work to validate this linear assumption in normal

tissue as well as diseased tissue is warranted to confirm and improve the dDSC diagnostic capability. In addition to validation of the linear assumption, other confounds to the BOLD signal, including the effects of vessel size, orientation, water diffusivity and the influence of hematocrit on BOLD signal variations,[55] need to be explored. The practicality of assessing the impact of these parameters *in vivo* is limited, but *in silico* validation using Monte Carlo simulation can explore the relationship between these parameters and the dDSC signal in future work.

This study has some notable limitations. Firstly, several confounds in the DSC model potentially affected the perfusion measurements in our dDSC technique, including delay and dispersion of bolus in the AIF. These confounds typically introduced errors in cases of severe vasculopathy, so they likely did not affect our cohort; however, application of dDSC to subjects with vascular disease will require technical improvement to address these issues, such as by modeling the vascular bed, extracting local AIF or using a delay-insensitive SVD-variant for perfusion quantification.[56–58] Secondly, these perfusion measurements showed large variability compared to ASL. However, previous comparison studies between ASL and gadolinium-based DSC have also demonstrated large variability.[59–61] And since this is a proof-of-concept study, our results demonstrated that the novel dDSC technique has the potential to measure blood flow, and that these measurements do vary proportionally with other conventional flow measurements like phase contrast and ASL.

Further optimization will be necessary to improve the quantitation and control for potential confounders such as breathing rate, minute ventilation and intra-subject variability in hypoxic exposure. Gaussian smoothing for noise reduction the BOLD datasets led to underestimated grey–white matter ratio in both CBF and CBV maps. Future work to optimize the hypoxic bolus depth and duration and use repeated hypoxic stimuli to improve signal-to-noise can require less spatial smoothing and increase grey–white matter perfusion differentiation. Even though repeatability tests showed reasonable performance on two healthy subjects (Supporting Information Figure S2), test-retest on a larger subset of subjects needs to be conducted for this methodology to better validate the diagnostic value of dDSC.

Another important limitation to our study is that a hypoxic stimulus may impact CBF in an unpredictable manner. Prolonged hypoxic exposure increases CBF,[62] but also causes hyperventilation that tends to counteract the hypoxic vasodilation.[62,63] Whether a challenge this brief raises or lowers CBF during the observation interval has not been determined since the transient duration of the hypoxia paradigm prevented measurement of CBF at steady-state hypoxia. A more in-depth and thorough investigation into stimulus-mediated changes in CBF is required to assess their contribution to our measurement uncertainty. Dual-acquisition of ASL and BOLD can be used to capture the dynamic BOLD signal as well as regional CBF changes across the brain during the hypoxia challenge; 4D-flow MRI can also be used to assess vasodilation in of the major arteries in the Circle of Willis in response to the hypoxic stimulus. Additionally, this experiment was originally designed with end-tidal O_2 and CO_2 acquisitions (Biopac Systems, Goleta, CA). However, during the course of the study, the gas sampling sensors broke, and we were not able to retrieve the end-tidal measurements. For future gas experiments, the use of a controlled respirator with prospective targeting of pO_2 and end-tidal CO_2 will be helpful to eliminate hypocapnia as a potential confounder.[64]

In conclusion, in this proof-of-concept study, we have demonstrated the feasibility of using transient hypoxia to generate a contrast bolus that mimics the effect of gadolinium and yields reasonable blood flow measurements. Even though our current dDSC implementation suffers from biases in perfusion estimates and requires further validation of its assumptions, dDSC still offers a novel gadolinium-free approach which will be attractive in pediatric and end-stage renal disease patients. Additionally, dDSC can be potentially beneficial for patients in whom serial DSC studies are required (such as in brain tumors), but this application awaits further investigation into the feasibility of dDSC in measuring impaired blood-brain barrier function. To improve the diagnostic utility of this method, block-design gas paradigms[65] and transfer function analysis[66] can be applied, and hypoxic stimuli can also be used in an interleaved manner with CO_2 inhalation to jointly estimate resting perfusion and cerebrovascular flow reserve. Since the AIF can easily be calculated in the heart and aorta, future studies can also extend this cerebral perfusion technique to blood flow measurements in other thoracic and abdominal organs.

Acknowledgments

The authors would like to acknowledge Mr. Bertin Valdez for his efforts coordinating the patient study visits and Dr. Thomas Coates, Dr. Tom Hofstra, Dr. Jackie Bascom, Susan Carson, Trish Peterson, and Debbie Harris from the CHLA Hematology Division for their assistance with patient recruitment.

Sources of funding

This work was supported by National Heart, Lung, and Blood Institute (grant 1U01-HL-117718-01, 1R01-HL136484-01A1 and a Minority Supplement to grant 1U01-HL-117718-01), the National Center for Research (5UL1-TR000130-05) through the Clinical Translational Science Institute at Children's Hospital Los Angeles, the National Institutes of Health (grant R01-NS074980), the National Institutes of Health Predoctoral Training in Interdisciplinary Neurosciences (1-T32-MH-111360-1-A1) and National Institute of Health grant (R01-ES024936). Philips Healthcare provided support for protocol development and applications engineering on a support-in-kind basis.

Declarations of interests

Chau Vu, Yaqiong Chai, Julie Coloigner, Aart Nederveen, Matthew Borzage, Adam Bush: none. John C. Wood: Research Funding NHLBI and NIDDK of the National Institutes of Health, Research Support-in-Kind from Philips Healthcare, Consultant for BluebirdBio, Celgene, Apopharma, WorldcareClinical, and BiomeInformatics.

References

1. Shiroishi MS, Castellazzi G, Boxerman JL, et al. Principles of T_2*-weighted dynamic susceptibility contrast MRI technique in brain tumor imaging. *J Magn Reson Imaging*. 2015;41(2):296-313. doi:10.1002/jmri.24648
2. Jahng G-H, Li K-L, Ostergaard L, Calamante F. Perfusion magnetic resonance imaging: a comprehensive update on principles and techniques. *Korean J Radiol*. 2014;15(5):554-577. doi:10.3348/kjr.2014.15.5.554
3. Yamada K, Wu O, Gonzalez RG, et al. Magnetic resonance perfusion-weighted imaging of acute cerebral infarction: effect of the calculation methods and underlying vasculopathy. *Stroke*. 2002;33(1):87-94. http://www.ncbi.nlm.nih.gov/pubmed/11779894. Accessed June 3, 2019.
4. Young GS. Advanced MRI of Adult Brain Tumors. *Neurol Clin*. 2007;25(4):947-973. doi:10.1016/j.ncl.2007.07.010
5. Beaumont A, Fatouros P, Gennarelli T, Corwin F, Marmarou A. Bolus tracer delivery measured by MRI confirms edema without blood-brain barrier permeability in diffuse traumatic brain injury. *Acta Neurochir Suppl*. 2006;96:171-174. http://www.ncbi.nlm.nih.gov/pubmed/16671449. Accessed June 3, 2019.
6. Agarwal R, Brunelli SM, Williams K, Mitchell MD, Feldman HI, Umscheid CA. Gadolinium-based contrast agents and nephrogenic systemic fibrosis: a systematic review and meta-analysis. *Nephrol Dial Transplant*. 2008;24(3):856-863. doi:10.1093/ndt/gfn593
7. Broome DR, Girguis MS, Baron PW, Cottrell AC, Kjellin I, Kirk GA. Gadodiamide-Associated Nephrogenic Systemic Fibrosis: Why Radiologists Should Be Concerned. *Am J Roentgenol*. 2007;188(2):586-592. doi:10.2214/AJR.06.1094
8. Murata N, Gonzalez-Cuyar LF, Murata K, et al. Macrocyclic and Other Non–Group 1 Gadolinium Contrast Agents Deposit Low Levels of Gadolinium in Brain and Bone Tissue. *Invest Radiol*. 2016;51(7):447-453. doi:10.1097/RLI.0000000000000252
9. McDonald RJ, McDonald JS, Kallmes DF, et al. Intracranial Gadolinium Deposition after Contrast-enhanced MR Imaging. *Radiology*. 2015;275(3):772-

782. doi:10.1148/radiol.15150025

10. Wáng Y-XJ, Schroeder J, Siegmund H, et al. Total gadolinium tissue deposition and skin structural findings following the administration of structurally different gadolinium chelates in healthy and ovariectomized female rats. *Quant Imaging Med Surg*. 2015;5(4):534-545. doi:10.3978/j.issn.2223-4292.2015.05.03
11. Losert C, Peller M, Schneider P, Reiser M. Oxygen-enhanced MRI of the brain. *Magn Reson Med*. 2002;48(2):271-277. doi:10.1002/mrm.10215
12. MacDonald ME, Berman AJL, Mazerolle EL, Williams RJ, Pike GB. Modeling hyperoxia-induced BOLD signal dynamics to estimate cerebral blood flow, volume and mean transit time. *Neuroimage*. 2018;178:461-474. doi:10.1016/j.neuroimage.2018.05.066
13. Chai Y, Bush AM, Coloigner J, et al. White Matter Has Impaired Resting Oxygen Delivery in Sickle Cell Patients. *Am J Hematol*. January 2019. doi:10.1002/ajh.25423
14. Bush AM, Borzage MT, Choi S, et al. Determinants of resting cerebral blood flow in sickle cell disease. *Am J Hematol*. 2016;91(9):912-917. doi:10.1002/ajh.24441
15. Borzage MT, Bush AM, Choi S, et al. Predictors of cerebral blood flow in patients with and without anemia. *J Appl Physiol*. 2016;120:976-981. doi:10.1152/japplphysiol.00994.2015
16. Alsop DC, Detre JA, Golay X, et al. Recommended implementation of arterial spin-labeled perfusion MRI for clinical applications: A consensus of the ISMRM perfusion study group and the European consortium for ASL in dementia. *Magn Reson Med*. 2015;73(1):102-116. doi:10.1002/mrm.25197
17. Peng S-L, Su P, Wang F-N, et al. Optimization of phase-contrast MRI for the quantification of whole-brain cerebral blood flow. *J Magn Reson Imaging*. 2015;42(4):1126-1133. doi:10.1002/jmri.24866
18. Østergaard L. Principles of cerebral perfusion imaging by bolus tracking. *J Magn Reson Imaging*. 2005;22(6):710-717. doi:10.1002/jmri.20460
19. Simonsen CZ, Ostergaard L, Vestergaard-Poulsen P, Røhl L, Bjørnerud A, Gyldensted C. CBF and CBV measurements by USPIO bolus tracking: reproducibility and comparison with Gd-based values. *J Magn Reson Imaging*.

1999;9(2):342-347. http://www.ncbi.nlm.nih.gov/pubmed/10077035. Accessed June 27, 2019.

20. Rosen BR, Belliveau JW, Vevea JM, Brady TJ. Perfusion imaging with NMR contrast agents. *Magn Reson Med*. 1990;14(2):249-265. http://www.ncbi.nlm.nih.gov/pubmed/2345506. Accessed April 22, 2019.
21. Chen JJ, Smith MR, Frayne R. The impact of partial-volume effects in dynamic susceptibility contrast magnetic resonance perfusion imaging. *J Magn Reson Imaging*. 2005;22(3):390-399. doi:10.1002/jmri.20393
22. Knutsson L, van Westen D, Petersen ET, et al. Absolute quantification of cerebral blood flow: correlation between dynamic susceptibility contrast MRI and model-free arterial spin labeling. *Magn Reson Imaging*. 2010;28(1):1-7. doi:10.1016/J.MRI.2009.06.006
23. Tudorica A, Fang Li H, Hospod F, et al. Cerebral blood volume measurements by rapid contrast infusion andT2*-weighted echo planar MRI. *Magn Reson Med*. 2002;47(6):1145-1157. doi:10.1002/mrm.10167
24. Rempp KA, Brix G, Wenz F, Becker CR, Gückel F, Lorenz WJ. Quantification of regional cerebral blood flow and volume with dynamic susceptibility contrast-enhanced MR imaging. *Radiology*. 1994;193(3):637-641. doi:10.1148/radiology.193.3.7972800
25. Østergaard L, Weisskoff RM, Chesler DA, Gyldensted C, Rosen BR. High resolution measurement of cerebral blood flow using intravascular tracer bolus passages. Part I: Mathematical approach and statistical analysis. *Magn Reson Med*. 1996;36(5):715-725. doi:10.1002/mrm.1910360510
26. Sangkatumvong S, Khoo MCK, Kato R, et al. Peripheral Vasoconstriction and Abnormal Parasympathetic Response to Sighs and Transient Hypoxia in Sickle Cell Disease. doi:10.1164/rccm.201103-0537OC
27. Coloigner J, Kim Y, Bush A, et al. Contrasting resting-state fMRI abnormalities from sickle and non-sickle anemia. Kassner A, ed. *PLoS One*. 2017;12(10):e0184860. doi:10.1371/journal.pone.0184860
28. Jenkinson M, Beckmann CF, Behrens TEJ, Woolrich MW, Smith SM. FSL. *Neuroimage*. 2012;62(2):782-790. doi:10.1016/J.NEUROIMAGE.2011.09.015

29. Bush A, Chai Y, Choi SY, et al. Pseudo continuous arterial spin labeling quantification in anemic subjects with hyperemic cerebral blood flow. *Magn Reson Imaging*. 2018;47:137-146. doi:10.1016/J.MRI.2017.12.011
30. Soares JM, Magalhães R, Moreira PS, et al. A Hitchhiker's Guide to Functional Magnetic Resonance Imaging. *Front Neurosci*. 2016;10:515. doi:10.3389/fnins.2016.00515
31. Mikl M, Mareček R, Hluštík P, et al. Effects of spatial smoothing on fMRI group inferences. *Magn Reson Imaging*. 2008;26(4):490-503. doi:10.1016/j.mri.2007.08.006
32. Lin W, Celik A, Derdeyn C, et al. Quantitative measurements of cerebral blood flow in patients with unilateral carotid artery occlusion: a PET and MR study. *J Magn Reson Imaging*. 2001;14(6):659-667. http://www.ncbi.nlm.nih.gov/pubmed/11747021. Accessed April 22, 2019.
33. Bulte D, Chiarelli P, Wise R, Jezzard P. Measurement of cerebral blood volume in humans using hyperoxic MRI contrast. *J Magn Reson Imaging*. 2007;26(4):894-899. doi:10.1002/jmri.21096
34. Grabner G, Janke AL, Budge MM, Smith D, Pruessner J, Collins DL. Symmetric atlasing and model based segmentation: an application to the hippocampus in older adults. *Med Image Comput Comput Assist Interv*. 2006;9(Pt 2):58-66. http://www.ncbi.nlm.nih.gov/pubmed/17354756. Accessed May 6, 2019.
35. Tatu L, Moulin T, Vuillier F, Bogousslavsky J. Arterial Territories of the Human Brain. In: *Frontiers of Neurology and Neuroscience*. Vol 30. ; 2012:99-110. doi:10.1159/000333602
36. Guensch DP, Fischer K, Yamaji K, et al. Effect of Hyperoxia on Myocardial Oxygenation and Function in Patients With Stable Multivessel Coronary Artery Disease. *J Am Heart Assoc*. 2020;9(5):e014739. doi:10.1161/JAHA.119.014739
37. Cox EF, Palaniyappan N, Aithal GP, Guha IN, Francis ST. Using MRI to study the alterations in liver blood flow, perfusion, and oxygenation in response to physiological stress challenges: Meal, hyperoxia, and hypercapnia. *J Magn Reson Imaging*. 2019;49(6):1577-1586. doi:10.1002/jmri.26341
38. Wengler K, Wang J, Serrano Sosa M, et al. Mapping hepatic blood oxygenation

by quantitative BOLD (qBOLD) MRI. *Magn Reson Med*. 2019;81(5):3272-3282. doi:10.1002/mrm.27642

39. van den Boomen M, Manhard MK, Snel GJH, et al. Blood oxygen level–dependent MRI of the myocardium with multiecho gradient-echo spin-echo imaging. *Radiology*. 2020;294(2):538-545. doi:10.1148/radiol.2020191845
40. Epstein FH, Meyer CH. Myocardial perfusion using arterial spin labeling CMR: promise and challenges. *JACC Cardiovasc Imaging*. 2011;4(12):1262-1264. doi:10.1016/j.jcmg.2011.08.015
41. Sangkatumvong S, Khoo MCK, Coates TD. Abnormal cardiac autonomic control in sickle cell disease following transient hypoxia. In: *2008 30th Annual International Conference of the IEEE Engineering in Medicine and Biology Society*. IEEE; 2008:1996-1999. doi:10.1109/IEMBS.2008.4649581
42. Bickler PE, Feiner JR, Lipnick MS, Batchelder P, MacLeod DB, Severinghaus JW. Effects of Acute, Profound Hypoxia on Healthy Humans. *Anesth Analg*. 2017;124(1):146-153. doi:10.1213/ANE.0000000000001421
43. van Osch MJP, van der Grond J, Bakker CJG. Partial volume effects on arterial input functions: Shape and amplitude distortions and their correction. *J Magn Reson Imaging*. 2005;22(6):704-709. doi:10.1002/jmri.20455
44. Hansen AE, Pedersen H, Rostrup E, Larsson HBW. Partial volume effect (PVE) on the arterial input function (AIF) in T_1 -weighted perfusion imaging and limitations of the multiplicative rescaling approach. *Magn Reson Med*. 2009;62(4):1055-1059. doi:10.1002/mrm.22098
45. Knutsson L, Börjesson S, Larsson E-M, et al. Absolute quantification of cerebral blood flow in normal volunteers: Correlation between Xe-133 SPECT and dynamic susceptibility contrast MRI. *J Magn Reson Imaging*. 2007;26(4):913-920. doi:10.1002/jmri.21093
46. Dolui S, Wang Z, Wang DJJ, et al. Comparison of non-invasive MRI measurements of cerebral blood flow in a large multisite cohort. *J Cereb Blood Flow Metab*. 2016;36(7):1244-1256. doi:10.1177/0271678X16646124
47. Knutsson L, Ståhlberg F, Wirestam R. Aspects on the accuracy of cerebral perfusion parameters obtained by dynamic susceptibility contrast MRI: a

simulation study. *Magn Reson Imaging*. 2004;22(6):789-798. doi:10.1016/J.MRI.2003.12.002

48. Juttukonda MR, Jordan LC, Gindville MC, et al. Cerebral hemodynamics and pseudo-continuous arterial spin labeling considerations in adults with sickle cell anemia. *NMR Biomed*. 2017;30(2):e3681. doi:10.1002/nbm.3681
49. Fields ME, Guilliams KP, Ragan DK, et al. Regional oxygen extraction predicts border zone vulnerability to stroke in sickle cell disease. *Neurology*. March 2018:10.1212/WNL.0000000000005194. doi:10.1212/WNL.0000000000005194
50. Mandell DM, Han JS, Poublanc J, et al. Selective Reduction of Blood Flow to White Matter During Hypercapnia Corresponds With Leukoaraiosis. *Stroke*. 2008;39(7):1993-1998. doi:10.1161/STROKEAHA.107.501692
51. Lu H, Clingman C, Golay X, van Zijl PCM. Determining the longitudinal relaxation time (T1) of blood at 3.0 Tesla. *Magn Reson Med*. 2004;52(3):679-682. doi:10.1002/mrm.20178
52. Wu W-C, Jain V, Li C, et al. In vivo venous blood T1 measurement using inversion recovery true-FISP in children and adults. *Magn Reson Med*. 2010;64(4):1140-1147. doi:10.1002/mrm.22484
53. Mark CI, Fisher JA, Pike GB. Improved fMRI calibration: Precisely controlled hyperoxic versus hypercapnic stimuli. *Neuroimage*. 2011;54(2):1102-1111. doi:10.1016/j.neuroimage.2010.08.070
54. Rostrup E, Larsson HB, Toft PB, Garde K, Henriksen O. Signal changes in gradient echo images of human brain induced by hypo- and hyperoxia. *NMR Biomed*. 1995;8(1):41-47. http://www.ncbi.nlm.nih.gov/pubmed/7547184. Accessed July 29, 2019.
55. Xu F, Li W, Liu P, et al. Accounting for the role of hematocrit in between-subject variations of MRI-derived baseline cerebral hemodynamic parameters and functional BOLD responses. *Hum Brain Mapp*. 2018;39(1):344-353. doi:10.1002/hbm.23846
56. Calamante F, Mørup M, Hansen LK. Defining a local arterial input function for perfusion MRI using independent component analysis. *Magn Reson Med*. 2004;52(4):789-797. doi:10.1002/mrm.20227

57. Mehndiratta A, Calamante F, Macintosh BJ, Crane DE, Payne SJ, Chappell MA. Modeling and correction of bolus dispersion effects in dynamic susceptibility contrast MRI. *Magn Reson Med*. 2014;72(6):1762-1774. doi:10.1002/mrm.25077
58. Wu O, Østergaard L, Weisskoff RM, Benner T, Rosen BR, Sorensen AG. Tracer arrival timing-insensitive technique for estimating flow in MR perfusion-weighted imaging using singular value decomposition with a block-circulant deconvolution matrix. *Magn Reson Med*. 2003;50(1):164-174. doi:10.1002/mrm.10522
59. Mutke MA, Madai VI, von Samson-Himmelstjerna FC, et al. Clinical evaluation of an arterial-spin-labeling product sequence in steno-occlusive disease of the brain. *PLoS One*. 2014;9(2):e87143. doi:10.1371/journal.pone.0087143
60. D'Ortenzio RM, Hojjat SP, Vitorino R, et al. Comparison of Quantitative Cerebral Blood Flow Measurements Performed by Bookend Dynamic Susceptibility Contrast and Arterial Spin-Labeling MRI in Relapsing-Remitting Multiple Sclerosis. *AJNR Am J Neuroradiol*. 2016;37(12):2265-2272. doi:10.3174/ajnr.A4939
61. Reginster P, Martin B, Denolin V. Comparative Study of Pseudo-Continuous Arterial Spin Labeling and Dynamic Susceptibility Contrast Imaging at 3.0 Tesla in Brain Tumors. 2017. https://www.semanticscholar.org/paper/Comparative-Study-of-Pseudo-Continuous-Arterial-and-Reginster-Martin/27d4956225eb94cc345f3eb3d6eeb4381123de58. Accessed October 16, 2019.
62. Xu F, Liu P, Pascual JM, Xiao G, Lu H. Effect of Hypoxia and Hyperoxia on Cerebral Blood Flow, Blood Oxygenation, and Oxidative Metabolism. *J Cereb Blood Flow Metab*. 2012;32(10):1909-1918. doi:10.1038/jcbfm.2012.93
63. LLOYD BB, JUKES MG, CUNNINGHAM DJ. The relation between alveolar oxygen pressure and the respiratory response to carbon dioxide in man. *Q J Exp Physiol Cogn Med Sci*. 1958;43(2):214-227. http://www.ncbi.nlm.nih.gov/pubmed/13542754. Accessed June 3, 2019.
64. Slessarev M, Han J, Mardimae A, et al. Prospective targeting and control of end-tidal CO2 and O2 concentrations. *J Physiol*. 2007;581(Pt 3):1207-1219. doi:10.1113/jphysiol.2007.129395

65. Dale AM, Buckner RL. Selective averaging of rapidly presented individual trials using fMRI. *Hum Brain Mapp*. 1997;5(5):329-340. doi:10.1002/(SICI)1097-0193(1997)5:5<329::AID-HBM1>3.0.CO;2-5

66. Duffin J, Sobczyk O, Crawley AP, Poublanc J, Mikulis DJ, Fisher JA. The dynamics of cerebrovascular reactivity shown with transfer function analysis. *Neuroimage*. 2015;114:207-216. doi:10.1016/j.neuroimage.2015.04.029

Figure Captions

Figure 1. Experimental setup for transient hypoxia gas paradigm and concurrent peripheral saturation S_pO_2 and MRI BOLD acquisitions. During the experiment, the subjects breathed through the mouthpiece through a two-liter reservoir rebreathing circuit that included one-way valves to prevent partial gas mixtures. The subject also wore a respiratory bellows to display the breathing pattern and frequency.

Figure 2. Transient hypoxia model. (**A**) Representative recording of S_pO_2 signal during 100% nitrogen paradigm. (**B**) S_pO_2 signal from the same patient prior to gas paradigm while patient was sleeping during anatomic scanning. (**C**) Representative time series of global BOLD-MR signal and S_pO_2 signals during hypoxia paradigm. (**D**) Representative ΔR_2^* time curve and its time integral (area under curve).

Figure 3. Localization of input functions from the difference image created by subtraction of baseline and hypoxic gradient-echo images. (**A**) Representative individual arterial input function (AIF) extracted from middle cerebral artery. (**B**) Representative individual venous output function (VOF) extracted from superior sagittal sinus. (**C**) Representative AIF and VOF during hypoxia demonstrated the process of rescaling the AIF by the time integral of the VOF to minimize partial volume effects.

Figure 4. Agreement between CBF_{dDSC} and alternative flow methods. (**A**) Correlation and (**B**) Bland-Altman analyses between CBF_{dDSC} and phase contrast flow. (**C**) Correlation and (**D**) Bland-Altman analyses between CBF_{dDSC} and ASL blood flow in the grey matter (GM). (**E**) Correlation and (**F**) Bland-Altman analyses between CBF_{dDSC} and ASL blood flow in the white matter (WM).

Figure 5. Group average perfusion and fit evaluation maps. (**A**) Cerebral blood flow (CBF), (**B**) cerebral blood volume (CBV), (**C**) mean transit time (MTT) and (**D**) root-mean-square percentage error (RMSPE) maps derived from the dDSC protocol. RMSPE

maps showed adherence to the *a priori* hypoxia model of linear rise and exponential decay.

Figure 6. Regional agreement between grey matter dDSC and ASL flow methods. Correlation and Bland-Altman analyses between grey matter CBF_{dDSC} and ASL blood flow in the (**A**, **B**) anterior cerebral artery territory (ACA), (**C**, **D**) middle cerebral artery territory (MCA) and (**E**, **F**) posterior cerebral artery territory (PCA).

Table Captions

Table 1. Patient demographic and baseline flow data. CBF was assessed using phase contrast (PC) and arterial spin labeling (ASL) in the grey matter (GM) and white matter (WM). Student's *t*-test was used to compare values between two groups. Values are reported as mean ± standard deviation. Bold letterings indicate statistical significance ($p<0.05$).

Table 2. Grey matter (GM), white matter (WM) and GM-WM ratio group average perfusion parameters. Students' *t*-test was used to compare values between two groups. Values are reported as mean ± standard deviation. Bold letterings indicate statistical significance ($p<0.05$).

Table 3. Group average dDSC perfusion parameters in different flow territories. Flow territories include territories perfused by the anterior cerebral arteries (ACA), middle cerebral arteries (MCA) and posterior cerebral arteries (PCA) in the grey matter. Values are reported as mean ± standard deviation.

Figures

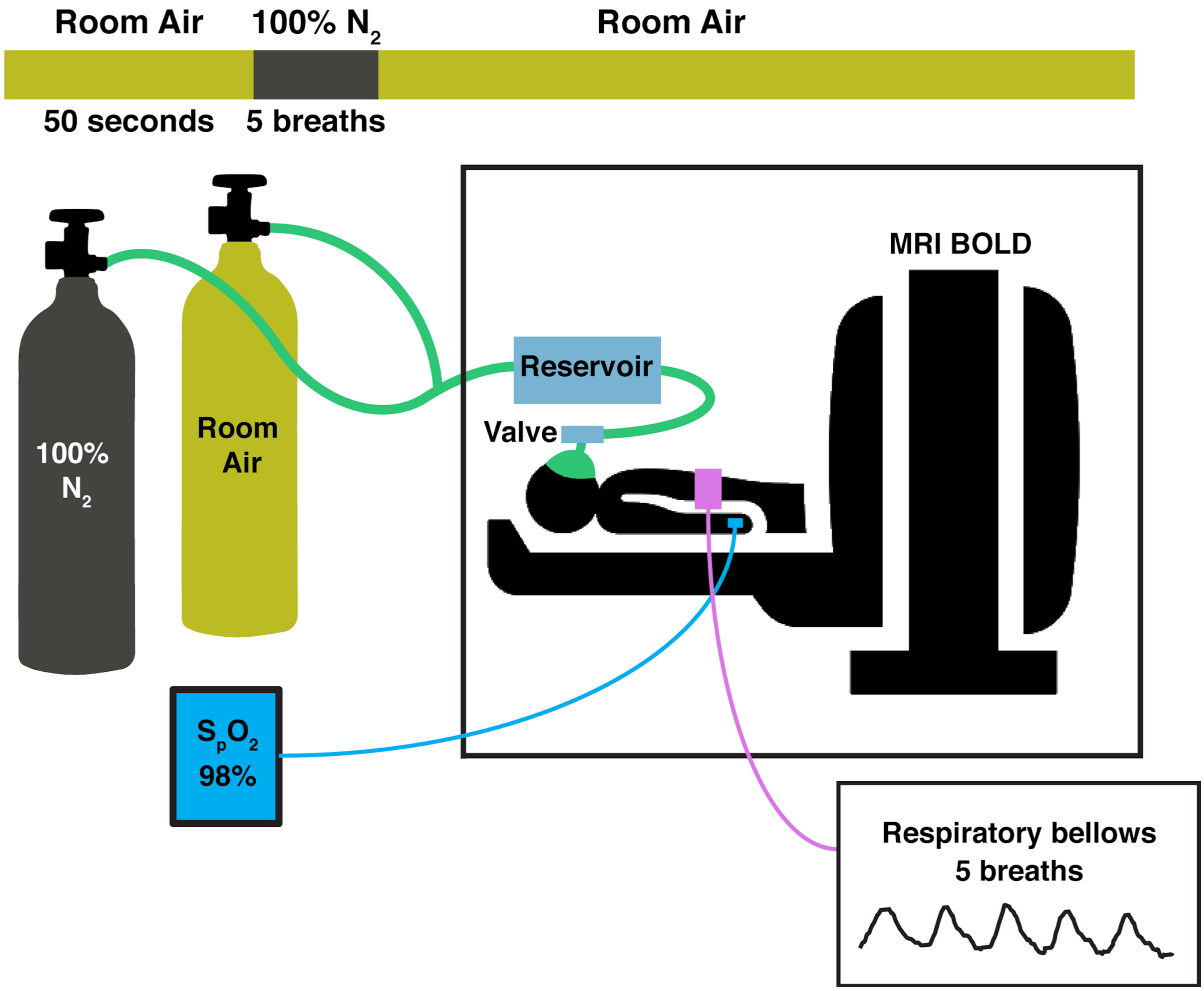

Figure 1. Experimental setup for transient hypoxia gas paradigm and concurrent peripheral saturation S_pO_2 and MRI BOLD acquisitions. During the experiment, the subjects breathed through the mouthpiece through a two-liter reservoir rebreathing circuit that included one-way valves to prevent partial gas mixtures. The subject also wore a respiratory bellows to display the breathing pattern and frequency.

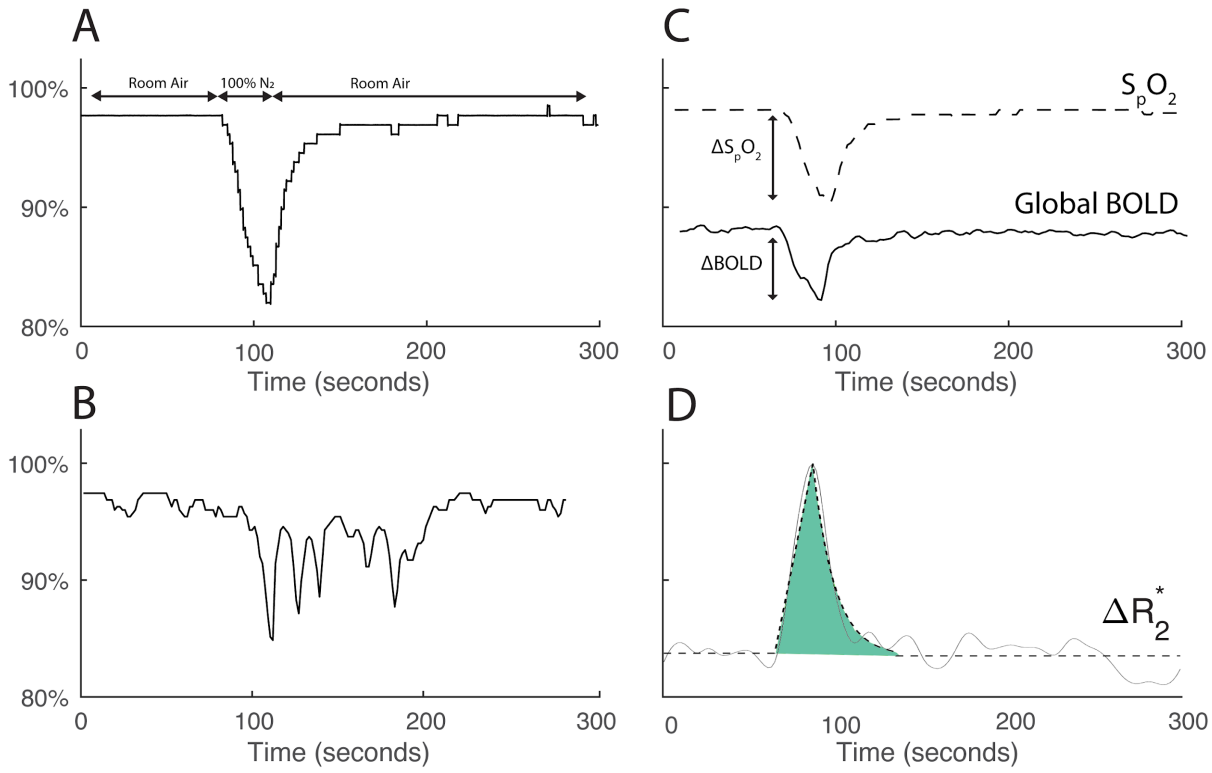

Figure 2. Transient hypoxia model. (A) Representative recording of S_pO_2 signal during 100% nitrogen paradigm. (B) S_pO_2 signal from the same patient prior to gas paradigm while patient was sleeping during anatomic scanning. (C) Representative time series of global BOLD-MR signal and S_pO_2 signals during hypoxia paradigm. (D) Representative ΔR_2^* time curve and its time integral (area under curve).

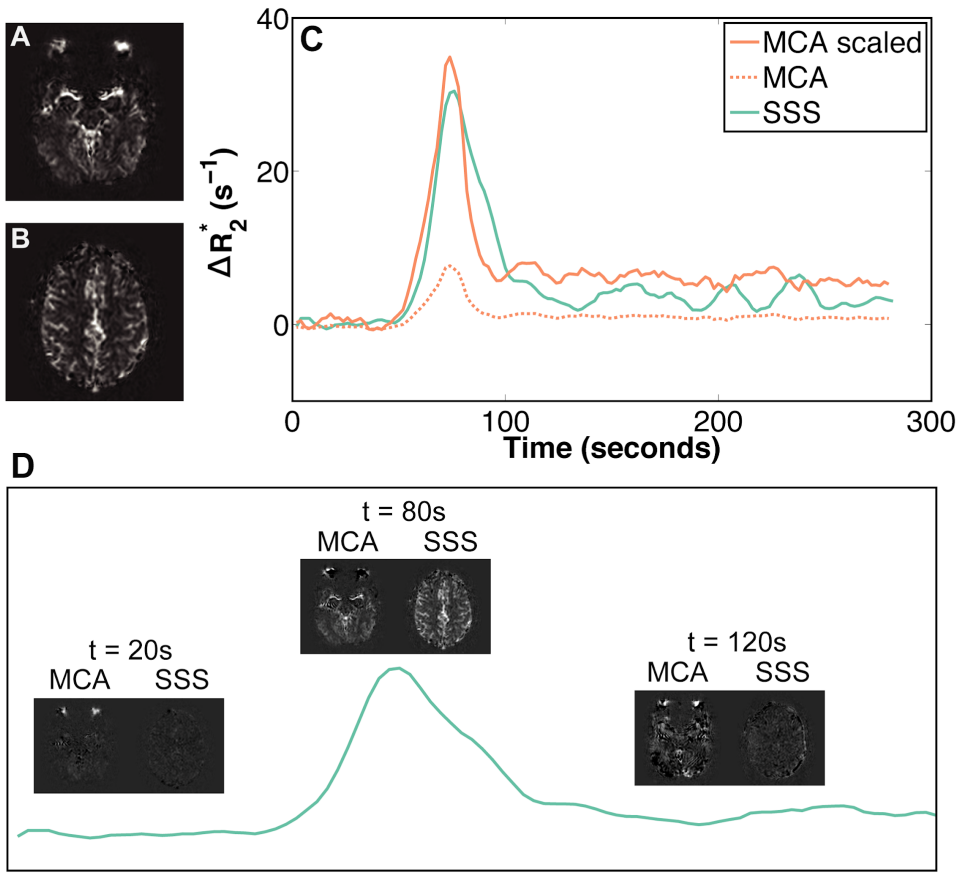

Figure 3. Localization of input functions from the difference image created by subtraction of baseline and hypoxic gradient-echo images. (A) Representative individual arterial input function (AIF) extracted from middle cerebral artery (MCA). (B) Representative individual venous output function (VOF) extracted from superior sagittal sinus (SSS). (C) Representative AIF, eAIF with venous scaling and VOF during hypoxia. (D) Motion-corrected simple difference from baseline signal at different time points during the hypoxia paradigm. The signals in the MCA and SSS were most visible at the peak of hypoxia.

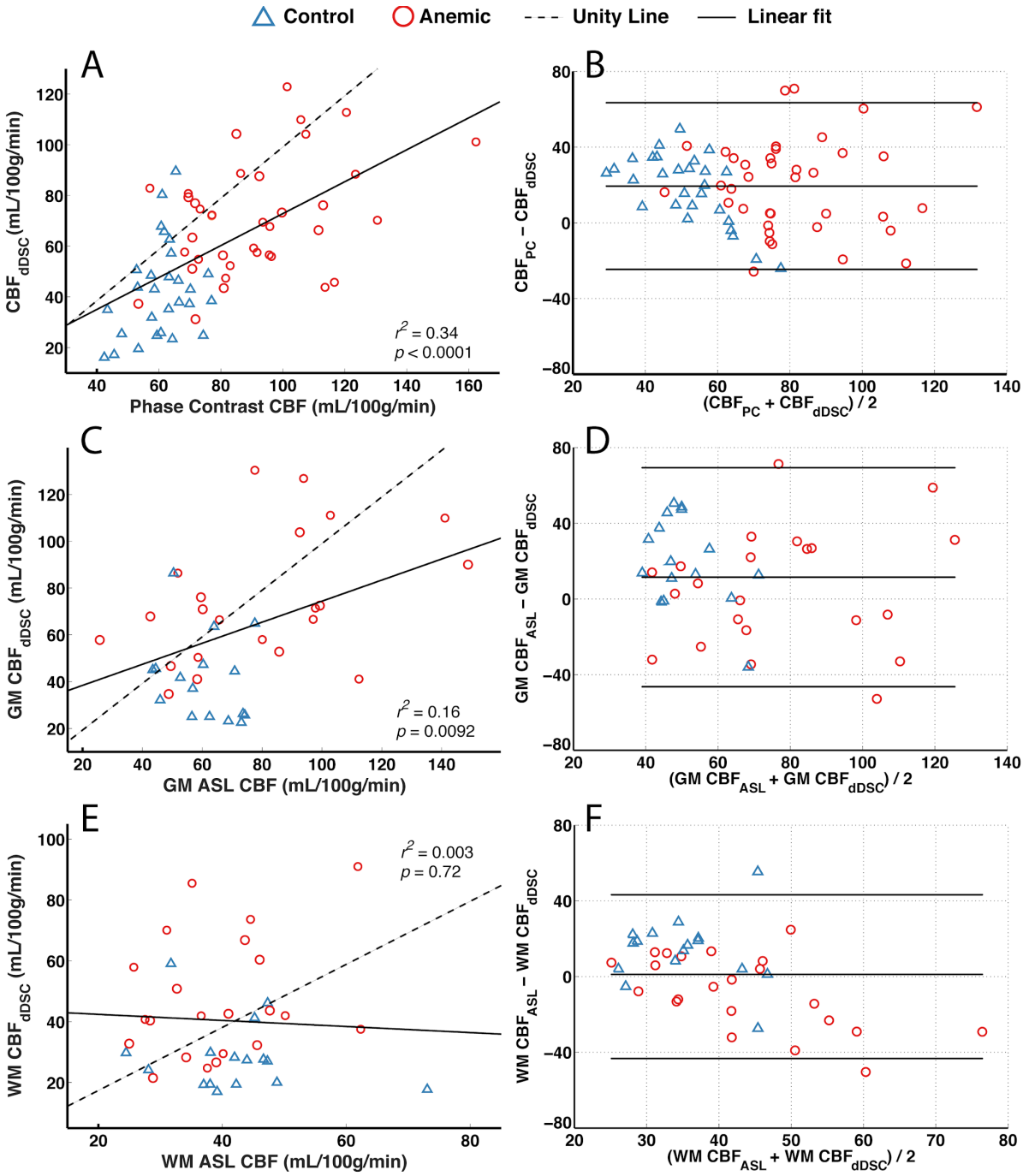

Figure 4. Agreement between CBF_{dDSC} and alternative flow methods. (A) Correlation and (B) Bland-Altman analyses between CBF_{dDSC} and phase contrast flow. (C) Correlation and (D) Bland-Altman analyses between CBF_{dDSC} and ASL blood flow in the grey matter (GM). (E) Correlation and (F) Bland-Altman analyses between CBF_{dDSC} and ASL blood flow in the white matter (WM).

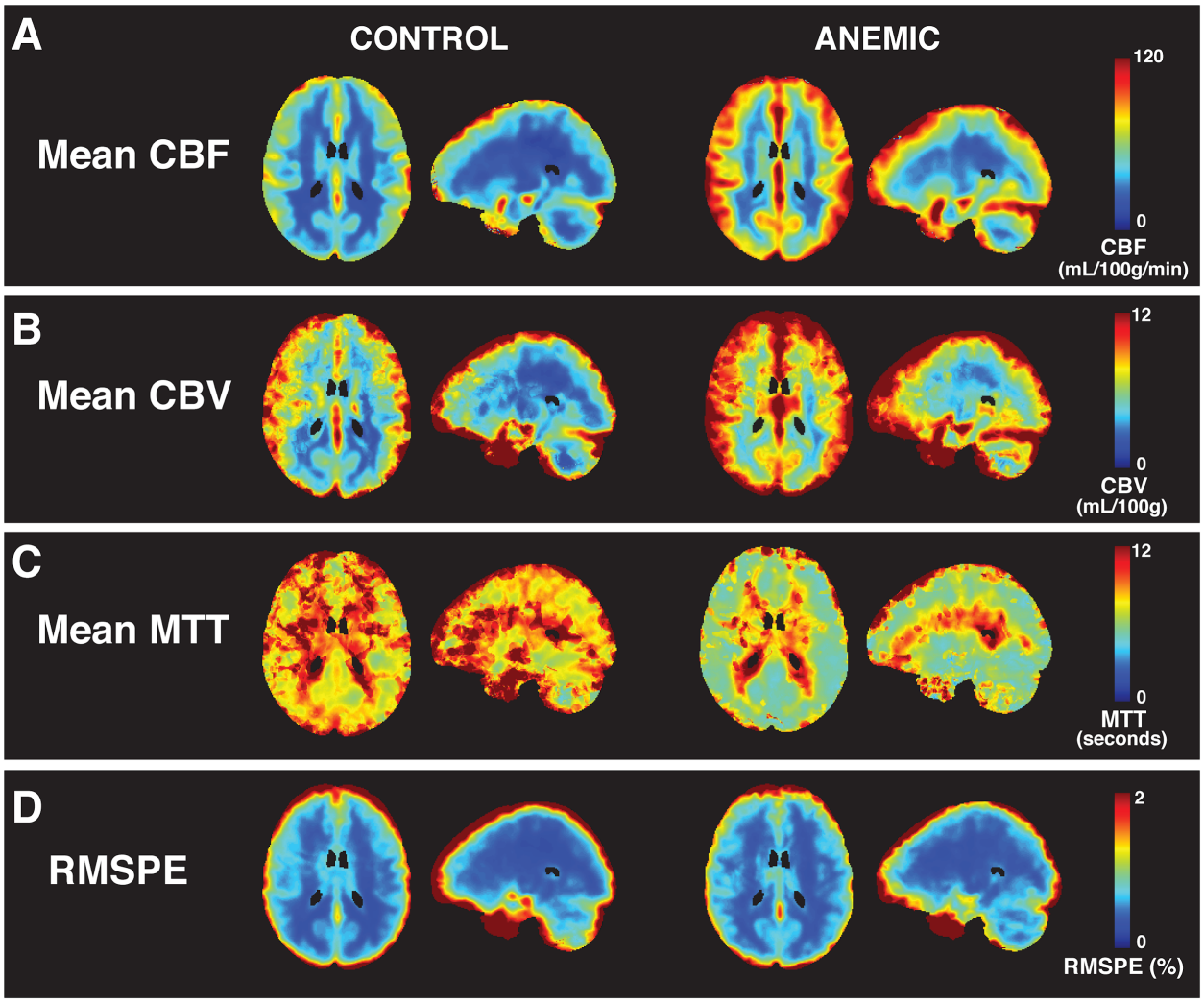

Figure 5. Group average perfusion and fit evaluation maps. (A) Cerebral blood flow (CBF), (B) cerebral blood volume (CBV), (C) mean transit time (MTT) and (D) root-mean-square percentage error (RMSPE) maps derived from the dDSC protocol. RMSPE maps showed adherence to the *a priori* hypoxia model of linear rise and exponential decay.

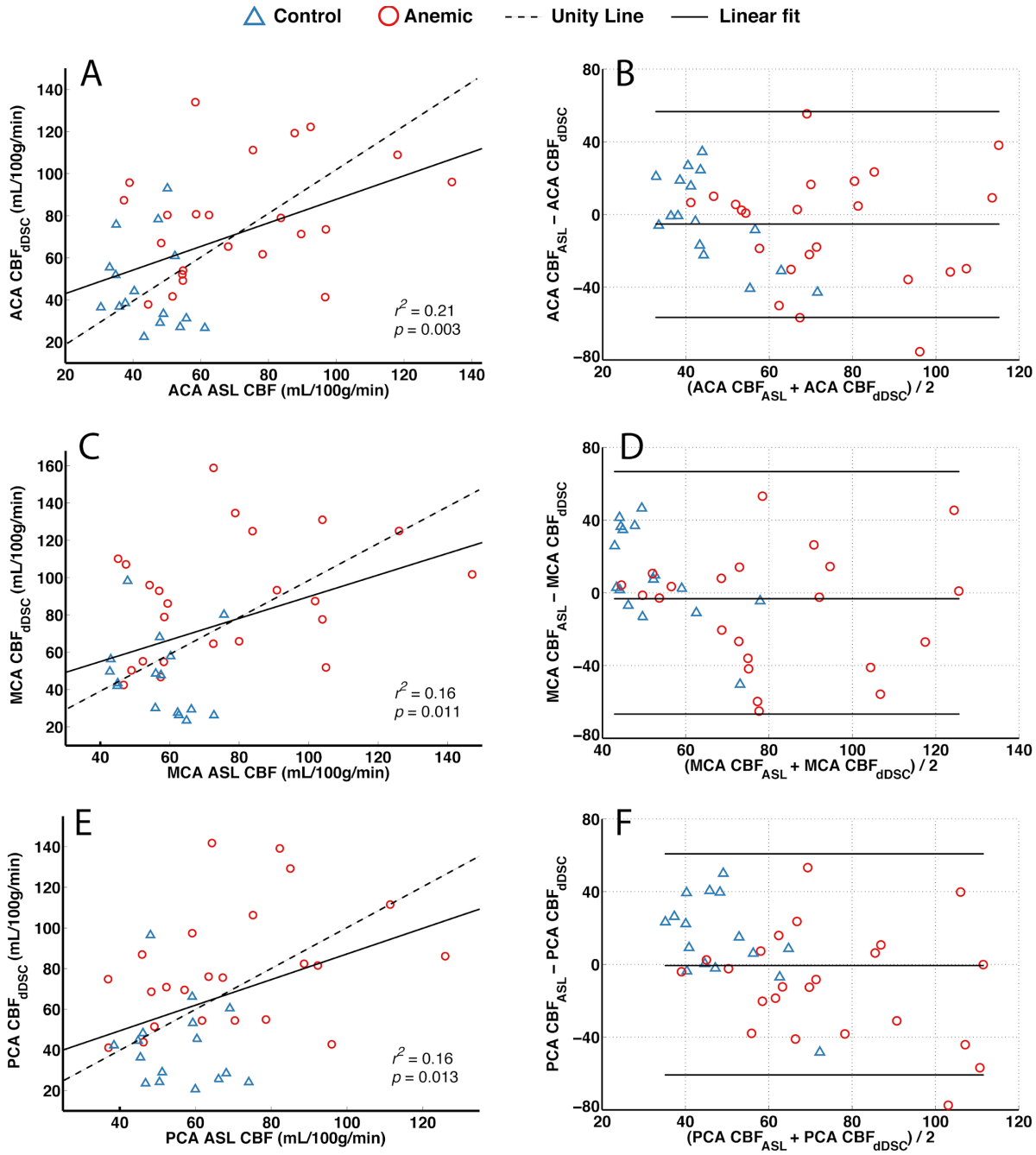

Figure 6. Regional agreement between grey matter dDSC and ASL flow methods. Correlation and Bland-Altman analyses between grey matter CBF_{dDSC} and ASL blood flow in the (A, B) anterior cerebral artery territory (ACA), (C, D) middle cerebral artery territory (MCA) and (E, F) posterior cerebral artery territory (PCA).

Tables

Table 1. Patient demographic and baseline flow data. CBF was assessed using phase contrast (PC) and arterial spin labeling (ASL) in the grey matter (GM) and white matter (WM). Demographics reflects the total cohort of 66 subjects in the PC comparative analysis and the reduced cohort of 41 subjects in the ASL analysis. Student's *t*-test was used to compare values between two groups. Values are reported as mean ± standard deviation. Bold letterings indicate statistical significance ($p<0.05$).

Phase contrast analysis	**Control** (N=28)	**Anemia** (N=38)	***p*-value**
Age (Years)	26.1±10.8	21.6±8.4	0.06
Sex	7M, 21F	17M, 21F	0.10
Hemoglobin (g/dL**)**	13.4±1.2	10.1±1.8	**<0.01**
Hematocrit (%)	39.7±3.4	29.5±5.0	**<0.01**
CBF_{PC} (mL/100g/min)	60.7±9.1	91.1±22.3	**<0.01**
ASL analysis	**Control** (N=16)	**Anemia** (N=25)	
Age (Years)	23.4±9.1	22.4±8.9	0.74
Sex	5M, 11F	10M, 15F	0.58
Hemoglobin (g/dL**)**	13.4±1.2	10.1±2.2	**<0.01**
Hematocrit (%)	40.1±3.8	29.8±5.9	**<0.01**
CBF_{ASL} GM (mL/100g/min)	60.9±11.4	77.3±30.0	**0.02**
CBF_{ASL} WM (mL/100g/min)	37.5±10.9	42.1±10.9	0.20

Table 2. Grey matter (GM), white matter (WM) and GM-WM ratio group average perfusion parameters. Students' *t*-test was used to compare values between two groups. Values are reported as mean ± standard deviation. Bold letterings indicate statistical significance ($p<0.05$).

	Control	**Anemia**	***p*-value**
CBF_{dDSC} GM (mL/100g/min)	41.3±17.5	70.8±24.9	**<0.01**
CBF_{dDSC} WM (mL/100g/min)	28.1±10.9	45.5±17.9	**<0.01**
CBF_{dDSC} GM/WM Ratio	1.5±0.2	1.6±0.1	**0.01**
CBV_{dDSC} GM (mL/100g)	4.6±1.5	6.2±1.4	**<0.01**
CBV_{dDSC} WM (mL/100g)	3.5±1.5	4.7±1.4	**<0.01**
CBV_{dDSC} GM/WM Ratio	1.4±0.2	1.4±0.2	0.74
MTT_{dDSC} GM (seconds)	8.5±1.9	7.5±1.9	**0.04**
MTT_{dDSC} WM (seconds)	8.4±2.0	7.3±1.7	**0.02**
MTT_{dDSC} GM/WM Ratio	1.0±0.1	1.0±0.1	0.16

Table 3. Group average dDSC perfusion parameters in different flow territories. Flow territories include territories perfused by the anterior cerebral arteries (ACA), middle cerebral arteries (MCA) and posterior cerebral arteries (PCA) in the grey matter. Values are reported as mean ± standard deviation.

	Control			**Anemia**		
	CBF (mL/100g/min)	**CBV** (mL/100g)	**MTT** (s)	**CBF** (mL/100g/min)	**CBV** (mL/100g)	**MTT** (s)
ACA	46.5±19.9	4.6±1.3	8.6±2.4	75.3±24.6	6.3±1.5	6.8±1.9
MCA	47.4±20.0	5.4±1.5	8.0±2.2	82.6±29.0	7.0±1.6	6.9±2.2
PCA	42.9±20.1	4.8±1.7	8.4±2.7	77.1±26.2	6.6±1.6	7.0±2.3

Supporting Information Figure Captions

Supporting Information Figure S1. Examples of individual perfusion maps in two representative control subjects and two representative anemic subjects. (**A**) Cerebral blood flow by dDSC (CBF_{dDSC}), (**B**) CBF by ASL (CBF_{ASL}) (**C**) cerebral blood volume (CBV_{dDSC}) and (**D**) mean transit time (MTT_{dDSC}). The ASL images were acquired at resolution = 3.7×3.7×10mm and then nonlinearly registered onto MNI template, so nonlinear warping could be seen on the sagittal plane.

Supporting Information Figure S2. Two repeated measurements of CBF, CBV and MTT maps on two healthy controls.

Supporting Information Table Captions

Supporting Information Table S1. Two repetitions of whole-brain perfusion measurements in two healthy controls.